

reported at coarser range resolution than the DOW data: 75 m for the DOW, 250 m for KLTX. Furthermore, the DOW oversampled azimuthally, calculating four beams per degree, whereas KLTX collected only one beam per degree. KLTX resolution was thus coarser than that of the DOW by a factor of 3.5 to 7. Because the roll wavelength was ~ 600 m with sub-roll peak wind speed regions with scales of ~ 100 m (Fig. 4), the rolls were less accurately characterized by KLTX and the peak wind intensity was underestimated. Peak-to-trough differences in wind speeds were near 10 m s^{-1} , only 30% of that observed by the DOW and lower than typical hurricane gust factors (16). An important consequence was that the KLTX data implied less severe peak low-level wind speeds than were observed at the ground or by the DOW (Fig. 6). Because the wind field sampled near KLTX had passed over ~ 40 km of land, some of the observed differences likely resulted from evolution of the near-surface wind field.

REFERENCES AND NOTES

1. R. Wakimoto and P. Black, *Bull. Am. Meteorol. Soc.* **75**, 189 (1994).
2. T. T. Fujita, *Storm Data* **34**, 25 (1992).
3. D. Jorgensen, *J. Atmos. Sci.* **41**, 1268 (1984).
4. ———, *ibid.*, p. 1287.
5. M. S. Powell, S. Houston, T. Reinhold, *Weather Forecast.* **11**, 329 (1996).
6. F. Marks Jr. and R. Houze Jr., *Bull. Am. Meteorol. Soc.* **65**, 569 (1984).
7. S. Stewart, J. Simpson, D. Wolff, in *22nd Conference on Hurricanes and Tropical Meteorology* (American Meteorological Society, Boston, 1997), p. 106.
8. J. Wurman, J. M. Straka, E. N. Rasmussen, *Science* **272**, 1774 (1996).
9. ———, M. Randall, A. Zahrai, *J. Atmos. Ocean. Tech.* **14**, 1502 (1997).
10. The DOW1 radar prototype described in (9) was upgraded to include a 2.44-m antenna, improved signal processing, and other hardware and software. The radar used a 40-kW transmitter operating at 9.375 GHz (32 mm). Pulses were 450 ns in duration, repeating every 500 μs , and sampled every 500 ns, resulting in range resolution of 75 m. The 2.44-m parabolic antenna produced a 0.95° beam, which spread to a width of 160 m at a range of 10 km from the radar. Radar beams were oversampled, resulting in 4 beams per degree.
11. This data collection mission was coordinated with the Hurricane Research Division (HRD) of the National Oceanic and Atmospheric Administration. F. Marks and S. Houston of HRD provided forecast guidance, other information, and coordination with the local weather service forecast office in Wilmington, NC. M. Biddle and C. Edwards, with J.W., crewed the DOW radar.
12. The Wilmington Weather Service Forecast Office provided real-time forecasting guidance and logistical support during the data collection. New Hanover International Airport provided the data site, logistics, and safety coordination during data collection. The taxiway was well removed from sources of airborne debris, particularly trees, tree limbs, and portions of damaged buildings. The tree line was generally 400 to 1000 m distant and blocked only the lowest radar beams, which were less than 1° above the horizon. The airport terminal building caused blockage up to several degrees above the horizon in the southern sector. Wetting of the antenna cover caused severe attenuation of both transmitted and received radiation, reducing sensitivity by 10 to 20 dB during periods

- of intense rainfall. Reflectivity and Doppler velocity data were collected in eight conical scans with inclinations ranging from 0° to 30° above the horizon, repeating every 300 s, to sample the volume of space surrounding the radar.
13. P. Dodge, S. Houston, J. Gamache, in (7), p. 115.
14. S. Houston, M. Powell, P. Dodge, *ibid.*, p. 92.
15. Data were translated, plotted, displayed, and gridded by the NCAR programs xltres, solo, reorder, and zeb, partially described in R. Oye and R. Carbone, in *20th Conference on Radar Meteorology* (American Meteorological Society, Boston, 1981), p. 683.
16. W. R. Krayer and R. D. Marshall, *Bull. Am. Meteorol. Soc.* **73**, 613 (1992).
17. T. Weckwerth, J. Wilson, R. Wakimoto, *Mon. Weather Rev.* **124**, 769 (1996).
18. T. Weckwerth, J. Wilson, R. Wakimoto, N. Crook, *ibid.* **125**, 505 (1997).
19. K. E. Emanuel, *Atmospheric Convection* (Oxford Univ. Press, New York, 1994).

20. T. Asai, *J. Meteorol. Soc. Jpn.* **48**, 18 (1970).
21. ———, *ibid.* **50**, 525 (1972).
22. J. Kuettnner, *Tellus* **23**, 404 (1971).
23. M. LeMone, *J. Atmos. Sci.* **30**, 1077 (1973).
24. A. Faller, *ibid.* **23**, 466 (1965).
25. W. Sun, *ibid.* **35**, 466 (1978).
26. R. Sykes and D. Henn, *ibid.* **46**, 1106 (1989).
27. R. Kropfli and N. Kohn, *J. Appl. Meteorol.* **17**, 669 (1978).
28. J. Kim and R. Moser, *J. Fluid Mech.* **177**, 133 (1987).
29. S. Kline, W. Reynolds, F. Schraub, P. Runstadler, *ibid.* **30**, 741 (1967).
30. Supported by the Cooperative Institute for Mesoscale Meteorological Studies and the School of Meteorology at the University of Oklahoma. The DOW radars are a collaborative effort among the University of Oklahoma, the National Center for Atmospheric Research, and the National Severe Storms Laboratory.

30 December 1997; accepted 19 February 1998

Switching Supramolecular Polymeric Materials with Multiple Length Scales

J. Ruokolainen, R. Mäkinen, M. Torkkeli, T. Mäkelä, R. Serimaa, G. ten Brinke,* O. Ikkala*

It was demonstrated that polymeric supramolecular nanostructures with several length scales allow straightforward tailoring of hierarchical order-disorder and order-order transitions and the concurrent switching of functional properties. Poly(4-vinyl pyridine) (P4VP) was stoichiometrically protonated with methane sulfonic acid (MSA) to form P4VP(MSA)_{1,0}, which was then hydrogen-bonded to pentadecylphenol. Microphase separation, re-entrant closed-loop macrophase separation, and high-temperature macrophase separation were observed. When MSA and pentadecylphenol were complexed to the P4VP block of a microphase-separated diblock copolymer poly[styrene-*block*-(4-vinyl pyridine)], self-organized structures-in-structures were obtained whose hierarchical phase transitions can be controlled systematically. This microstructural control on two different length scales (in the present case, at 48 and 350 angstroms) was then used to introduce temperature-dependent transitions in electrical conductivity.

During the past decade, methods to prepare nanosized structures have progressed greatly, stimulated by the continuing demand for miniaturization of devices and electronic components. Polymers offer a means to construct ordered nanoscale domains through self-organization, on the basis of competing interactions (1–7). Perhaps the most studied example is provided by block copolymers, where the repulsion between the chemically connected blocks leads to self-organization into lamellar, cylindrical, spherical, and other structures

with length scales on the order of 100 to 1000 Å (1). Even more complicated structures have been created with block copolymers containing rigid moieties (4, 8). Recently, another concept to achieve mesomorphic structures at much smaller length scales (typically 30 to 40 Å) has been presented in which nonmesogenic amphiphilic oligomers are noncovalently bonded to homopolymers (5, 6, 9). In the case of hydrogen bonding between amphiphilic oligomers such as pentadecylphenol (PDP) and homopolymers such as P4VP, the competition between attraction and repulsion leads to a microphase-separated (often lamellar) morphology at low temperatures (6, 10, 11). Heating yields an order-disorder transition to a disordered phase (10, 11).

Here, we show that the two above-mentioned ordering principles can be combined with the use of diblock copolymers consisting of a coil-like block and a block consisting of a supramolecular polymer-amphiphile complex, allowing microstructural control on two length scales. The hierarchi-

J. Ruokolainen and O. Ikkala, Department of Engineering Physics and Mathematics, Helsinki University of Technology, FIN-02015 HUT, Espoo, Finland.

R. Mäkinen, M. Torkkeli, R. Serimaa, Department of Physics, University of Helsinki, Post Office Box 9, FIN-00014, Helsinki, Finland.

T. Mäkelä, VTT Microelectronics, Technical Research Centre of Finland, Post Office Box 1101, FIN-02044 VTT, Espoo, Finland.

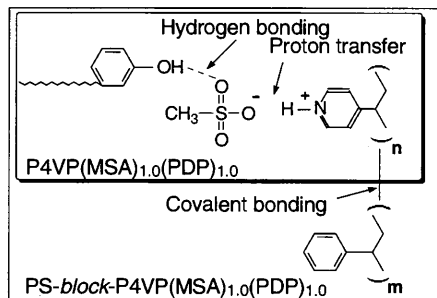
G. ten Brinke, Department of Polymer Science and Materials Science Center, University of Groningen, Nijenborgh 4, 9747 AG Groningen, Netherlands.

*To whom correspondence should be addressed. E-mail: G.ten.Brinke@chem.rug.nl; Olli.Ikkala@hut.fi

cal nanostructures were imaged, and it is shown that functionalization of one block results in transitions in electrical conductivity that can be explained by dimensionality transitions.

P4VP was first protonated with methane sulfonic acid (MSA). Fourier transform infrared measurements (FTIR) indicate (12) that a nominally complete protonation was achieved once the number of MSA molecules equaled or exceeded the number of pyridine groups. The resulting polysalt, denoted here as P4VP(MSA)_{1.0}, was then mixed with PDP, which forms hydrogen bonds to the sulfonate group. Because of the large absorption bandwidth of the sulfonate regime, FTIR does not easily lend itself to detailed investigation of such hydrogen bonding. However, calculations of hydrogen-bonded complexes of sulfuric acid and water (13) suggest that the hydrogen bonding between the phenolic hydroxyl group and the sulfonate group of MSA becomes energetically feasible once a proton has been transferred from MSA to P4VP. Thus,

the expected supramolecular structure combines proton transfer and hydrogen bonding (Scheme 1). Nominally one PDP molecule is used for each sulfonate group, but the actual number of PDP molecules that are hydrogen bonded remains uncertain at present.



Scheme 1.

Optical microscopy shows a complex phase behavior for P4VP(MSA)_{1.0}(PDP)_{1.0} consisting of optically anisotropic, transparent, and cloudy phases (Fig. 1). To identify the phases, we conducted small-angle x-ray measurements (SAXS) as a function of temperature, using methods described elsewhere (11). Below 100°C, a distinct and relatively narrow SAXS peak at the scattering vector $q \approx 0.13 \text{ \AA}^{-1}$ was observed, corresponding to a lamellar structure with a long period of $L_c \approx 48 \text{ \AA}$ (14). Above 100°C, a steplike increase in the half-width of this Bragg reflection was observed. In close analogy with conventional block copolymers (15), a broad correlation hole peak remained visible, which upon further heating gradually decreased and shifted to a smaller angle, as a result of the reduction in the number of hydrogen bonds. Near 175°C, a strong forward scattering peak appeared, signaling macrophase separation. The intensity of this peak diminished again above ~200°C. The phase separation at ~220°C could not be identified in the SAXS data.

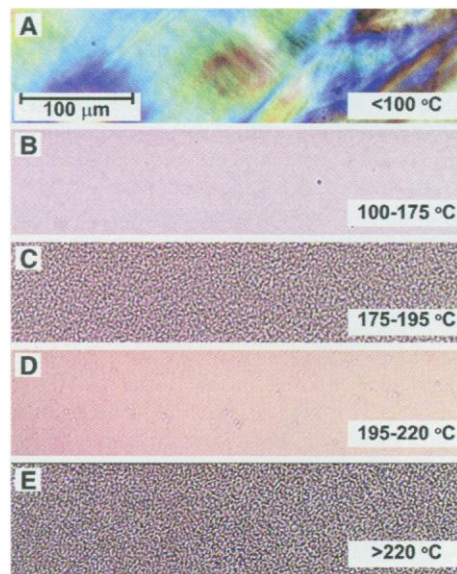


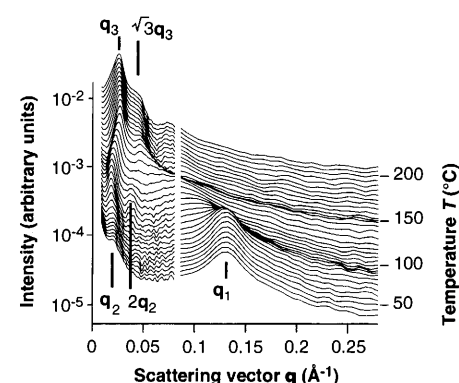
Fig. 1. Optical micrographs illustrating the phase behavior of P4VP(MSA)_{1.0}(PDP)_{1.0}. (A) An optically anisotropic texture is observed below ~100°C with crossed polarizers. (B) Above 100°C, the sample becomes transparent, indicating a homogeneous (disordered) phase up to ~175°C. (C) Between 175° and 195°C, the sample becomes cloudy, indicating macrophase separation. Because MSA does not phase separate from P4VP at these temperatures (12), it is evident that PDP molecules will be decoupled from the P4VP(MSA)_{1.0} backbone because of the reduced hydrogen-bonding strength. (D) Further heating causes the sample to become homogeneous again [re-entrant phase behavior (24)]. (E) Eventually, above ~220°C, most of the PDP molecules separate again from the rest of the system, which is the usual lower critical solution temperature behavior of polymer systems (25).

Fig. 2. SAXS intensity curves of PS-block-P4VP(MSA)_{1.0}(PDP)_{1.0} during heating at 2°C/min. Near room temperature, two peaks are present: $q_2 \approx 0.017 \text{ \AA}^{-1}$ and $q_1 \approx 0.13 \text{ \AA}^{-1}$. Additionally, $2q_2$ becomes distinct near 90°C when the rubbery state of PS allows better ordering. Therefore, the structure consists of alternating layers of PS and P4VP(MSA)_{1.0}(PDP)_{1.0}. The peak at q_1 corresponds to lamellar order within the P4VP(MSA)_{1.0}(PDP)_{1.0} layers. It is at the same position as for the corresponding homopolymer complex, that is, P4VP(MSA)_{1.0}(PDP)_{1.0}, where a small second-order peak could still be resolved at $2q_1$. Near 100°C, the peak at q_1 suddenly broadens and decreases because the lamellar structure within P4VP(MSA)_{1.0}(PDP)_{1.0} layers disappears because of an order-disorder transition (ODT_c). Near 150°C, the peaks at q_2 and $2q_2$ are replaced by peaks at $q_3 \approx 0.026 \text{ \AA}^{-1}$ and $\sqrt{3} q_3$, signaling an order-order transition (OOT_b) from a lamellar to a cylindrical morphology.

Hence, supramolecular P4VP(MSA)_{1.0}(PDP)_{1.0} structures show mesomorphic order at a short length scale L_c , as well as a sequence of phase transitions. In a next step, we confined this system inside another nanostructure with a longer length scale L_b by using diblock copolymers in which the P4VP chains form the minority blocks of microphase-separating diblock copolymers of polystyrene (PS) and P4VP, PS-*block*-P4VP. The number-averaged molecular masses of the P4VP and PS blocks were selected to be 5600 and 40,000 daltons, respectively, resulting in a spherical morphology for the uncomplexed PS-*block*-P4VP system, as confirmed by SAXS and transmission electron microscopy (TEM) (16). This finding is in perfect agreement with the volume fraction of the P4VP blocks, $f = 0.12$. Classically, an increase of f yields a transition to the cylindrical ($f = 0.16$) and lamellar ($f = 0.32$) phases (17). MSA and PDP act as selective solvents for the P4VP domains, and the complexation of MSA and PDP to the pyridine blocks introduces a simple way to control the phase morphology because the volume fraction of the P4VP-containing domains can be controlled effectively. In this way, supramolecular structures combining covalent bonding, proton transfer, and hydrogen bonding were obtained (Scheme 1). Judicious selection of the block lengths (n and m), the length of the phenolic alkyl group, and also the sulfonic acid thus allows a detailed tailoring of hierarchical self-organized structures, as will subsequently be discussed in one particular case.

The SAXS data (Fig. 2) for PS-*block*-P4VP(MSA)_{1.0}(PDP)_{1.0} as a function of temperature show three regimes:

1) Below ~100°C (Figs. 2 and 3A), the P4VP(MSA)_{1.0}(PDP)_{1.0} and PS blocks formed alternating layers with a long period $L_b \approx 350 \text{ \AA}$. A lamellar morphology could be expected because the volume of P4VP(MSA)_{1.0}(PDP)_{1.0} divided by the to-



tal volume corresponds to $f = 0.40$, given the assumption that both MSA and PDP are nominally fully complexed to P4VP. The $P4VP(MSA)_{1.0}(PDP)_{1.0}$ layers were further microphase separated into another lamellar structure with a long period $L_c \approx 48 \text{ \AA}$. In a separate study involving a closely related system of PS-*block*-P4VP fully complexed with nonadecylphenol, which has a longer alkyl tail than PDP, we were able to resolve these mutually perpendicular lamellar structures by TEM (Fig. 4).

2) Between 100°C and 150°C (Figs. 2 and 3B), the $P4VP(MSA)_{1.0}(PDP)_{1.0}$ and PS blocks continued to form a lamellar structure, but the second layered structure had disappeared. Therefore, an order-disorder transition within the polymer-amphiphile complex layers took place at 100°C .

3) Above $\sim 150^\circ\text{C}$ (Figs. 2 and 3C), the disordered $P4VP(MSA)_{1.0}(PDP)_x$ ($x \ll 1$) domains formed hexagonal cylindrical

structures within the rest of the material, that is, PS and part of PDP. This transition is due to the fact that PDP became miscible with PS above about 130°C (16) and that, as discussed above, the hydrogen bonding between PDP and $P4VP(MSA)_{1.0}$ diminished strongly at increased temperatures [eventually leading to macrophase separation in the homopolymer case (Fig. 1)]. This result implies that PDP will decouple from the $P4VP(MSA)_{1.0}$ backbone and gradually diffuse into the PS phase, thus effectively increasing the volume fraction of the PS-containing domains at the cost of the $P4VP(MSA)_{1.0}$ -containing domains. A complete transition of PDP to the PS domains would correspond to a volume fraction for $P4VP(MSA)_{1.0}$ of $f = 0.21$, far inside the cylindrical morphology regime. Therefore, an order-order transition took place at the block copolymer length scale at 150°C .

We now turn to the question of how these transitions manifest themselves in the (protonic) conductivity. Ac impedance measurements of the pure polysalt $P4VP(MSA)_{1.0}$ (Fig. 5) suggest that the conductivity σ is governed by a single activation energy in analogy with the results for sulfuric acid-complexed polyethylene imine (18). Compared with $P4VP(MSA)_{1.0}$, a qualitatively different behavior was observed for $P4VP(MSA)_{1.0}(PDP)_{1.0}$. In this case, the macrophase separation manifested itself in a decrease in the conductivity. Finally, we considered the PS-*block*- $P4VP(MSA)_{1.0}(PDP)_{1.0}$ sys-

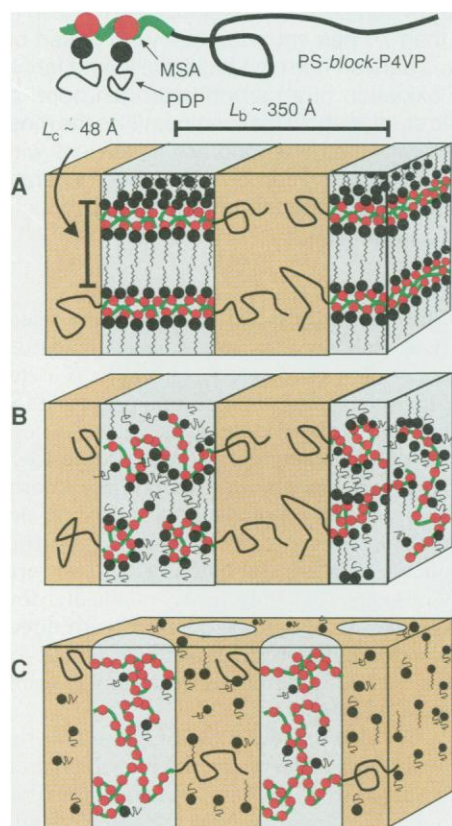


Fig. 3. Schematic illustration of the self-organized structures of PS-*block*- $P4VP(MSA)_{1.0}(PDP)_{1.0}$. The local structures are indicated; macroscopically, the samples are isotropic. (A) Alternating PS layers and layers consisting of alternating one-dimensional slabs of $P4VP(MSA)_{1.0}$ and PDP for $T < T_{ODT_c}$ (14). (B) Alternating two-dimensional PS and disordered $P4VP(MSA)_{1.0}(PDP)_{1.0}$ lamellae for $T_{ODT_c} < T < T_{OOT_b}$. (C) One-dimensional disordered $P4VP(MSA)_{1.0}(PDP)_x$ (with $x \ll 1$) cylinders within the three-dimensional PS-PDP medium for $T > T_{OOT_b}$.

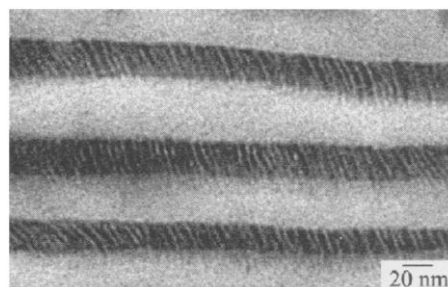


Fig. 4. Transmission electron micrograph of PS-*block*- $P4VP(NPD)_{1.0}$, where nominally one nonadecylphenol (NPD) has been hydrogen bonded with each pyridine group. The long period of the alternating PS (light grey) and $P4VP(NPD)_{1.0}$ (dark grey) lamellae equals $L_b \approx 550 \text{ \AA}$. It is slightly larger than in the other samples of this work because of the higher molecular mass of this particular sample. The number-averaged molecular masses of the P4VP and PS blocks were 49,500 and 238,000 daltons, respectively. The $P4VP(NPD)_{1.0}$ lamellae are further ordered into alternating lamellae of nonpolar nonadecyl tails of NPD molecules and polar P4VP backbones. The long period of this structure is $L_c \approx 40 \text{ \AA}$. The two sets of lamellar structures are, as expected, mutually perpendicular.

tem (Fig. 5). For temperature $T < T_{ODT_c}$, the sample consisted of conducting nanoscale slabs separated by insulating PS and PDP domains (Fig. 3A). Therefore, locally, the conductivity was highly anisotropic, taking place in one direction only. No effort was made to orient the microphase-separated domains macroscopically, and therefore only a small macroscopic conductivity was observed because of averaging over all directions. The order-disorder transition inside the $P4VP$ -containing layers resulted in conducting lamellae, with local conductivity taking place in two dimensions. Macroscopically, this transition was accompanied by an order of magnitude increase in the conductivity. Finally, above the order-order transition, the local conductivity again took place in one direction only, leading to a reduction in the conductivity (Fig. 5). Thus, it is demonstrated that the control of the microstructure allows a means to control the macroscopic conductivity. Drastically larger anisotropic effects ac-

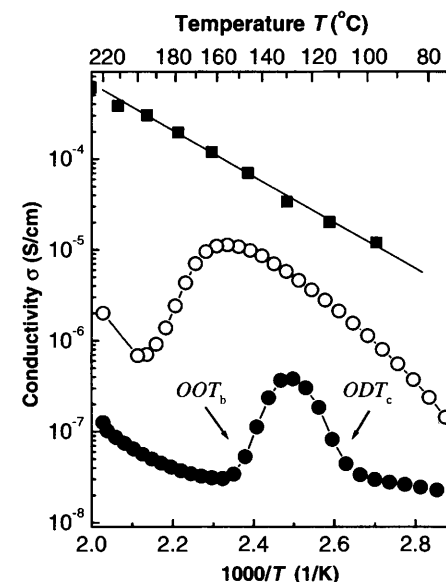


Fig. 5. Electrical conductivity (σ) during heating at $5^\circ\text{C}/\text{min}$, on the basis of ac impedance measurements extrapolated to zero frequency. Similar data are observed during cooling. ■, $P4VP(MSA)_{1.0}$ showing the classical thermally activated conductivity; ○, $P4VP(MSA)_{1.0}(PDP)_{1.0}$ showing thermally activated behavior up to $\sim 160^\circ\text{C}$, at which the first signals of imminent macrophase separation appear. A further increase in temperature results in a decrease in σ . The conductivity starts to increase again above $\sim 195^\circ\text{C}$. ●, PS-*block*- $P4VP(MSA)_{1.0}(PDP)_{1.0}$, where the order-disorder transition (ODT_c) within the $P4VP(MSA)_{1.0}(PDP)_{1.0}$ domain and order-order transition (OOT_b) at the block copolymer length scale are distinctively present in the conductivity. The samples have not been oriented, and therefore the results represent averages over all directions. The lines are drawn only to guide the eye.

companying the dimensionality transitions are expected, eventually approaching on-off switching, once efforts are taken to orientate the nanostructures.

The implications of the present work on nanotechnology seem manifold. The present methods to construct zero-, one-, and two-dimensional nanostructures suggest controllable nanostructures in conjugated electronically conducting polymers. P4VP is a semiconducting side-chain-conjugated polymer. In this case, conductivity appears to proceed through a protonic mechanism (19); this mechanism is not a serious limitation to the generality of the concepts, which are based on a control of the morphology. Chemically, P4VP resembles in several ways main-chain-conjugated polymers such as polyaniline, poly(*p*-pyridine), poly(*p*-pyridine vinylene) (20, 21), and possibly even polypyrrole. These materials are inherently difficult to process because of their rigidity. However, in polyaniline, for example, methods have been demonstrated to introduce processibility by the use of amphiphilic dopants (22) or amphiphilic oligomers capable of molecular recognition with the polyaniline chain (23). Such concepts easily provide the short length scale discussed above.

REFERENCES AND NOTES

1. F. S. Bates and G. H. Fredrickson, *Annu. Rev. Phys. Chem.* **41**, 525 (1990).
2. M. Muthukumar, C. K. Ober, E. L. Thomas, *Science* **277**, 1225 (1997).
3. C. K. Ober and G. Wegner, *Adv. Mater.* **9**, 17 (1997).
4. S. I. Stupp *et al.*, *Science* **276**, 384 (1997).
5. M. Antonietti, J. Conrad, A. Thümmann, *Trends Polym. Sci.* **5**, 262 (1997).
6. G. ten Brinke and O. Ikkala, *ibid.*, p. 213.
7. M. Park, C. Harrison, P. M. Chaikin, R. A. Register, D. H. Adamson, *Science* **276**, 1401 (1997).
8. Diblock copolymers consisting of chemically connected side-chain liquid crystalline and flexible blocks yielding self-organization at two length scales are described by, for example, M. Yamada, I. Tsukasa, A. Hirao, S. Nakahama, and J. Watanabe [*Macromolecules* **28**, 50 (1995)], G. Mao *et al.* [*ibid.* **30**, 2556 (1997)], H. Fischer and S. Poser [*Acta Polym.* **47**, 413 (1996)], and G. Mao and C. K. Ober [*ibid.* **48**, 405 (1997)]. Compared with our work, the structure formation in such materials invokes an additional ordering principle because the short length scale results from the mesogenic nature of the side chains.
9. G. Wegner, *Makromol. Chem. Macromol. Symp.* **1**, 151 (1986).
10. J. Ruokolainen *et al.*, *Phys. Rev. E* **54**, 6646 (1996).
11. J. Ruokolainen *et al.*, *Macromolecules* **30**, 2002 (1997).
12. The ionic bonding of MSA to P4VP can be monitored by the use of the characteristic FTIR absorption band at 1637 cm^{-1} of the quaternized pyridine ring as compared with the corresponding free pyridine ring at 1597 cm^{-1} [J. Ruokolainen *et al.*, *Macromolecules* **29**, 6621 (1996)].
13. H. Arstila, K. Laasonen, A. Laaksonen, *J. Chem. Phys.* **108**, 1031 (1998).
14. The two levels of structure are distinguished by their subscripts. For example, the long period for the mesomorphic polymer-amphiphile structure is denoted as L_c and the long period for the block copolymer

length scale as L_b . Similarly, the order-disorder transition for the polymer-amphiphile complex is denoted as ODT_c and the order-order transition in block copolymer length scale as OOT_b .

15. P.-G. de Gennes, *Scaling Concepts in Polymer Physics* (Cornell Univ. Press, Ithaca, NY, 1979).
16. M. Saariaho *et al.*, in preparation.
17. L. Leibler, *Macromolecules* **13**, 1602 (1980).
18. M. F. Daniel, B. Desbat, F. Cruège, O. Trinquet, J. C. Lassegues, *Solid State Ionics* **28-30**, 637 (1988).
19. The motivation to protonate side chain-conjugated P4VP by MSA originates from previous studies: The main chain-conjugated polyaniline can be doped to yield electronic conductivity by protonating the iminic nitrogens with stoichiometric amounts of strong acids [J.-C. Chiang and A. G. MacDiarmid, *Synth. Met.* **13**, 193 (1986)]. The amines of polyethylene imine can be protonated by stoichiometric amounts of sulfuric or phosphoric acid to yield protonic conductivity (18).

20. Y. Z. Wang *et al.*, *Synth. Met.* **84**, 1179 (1997).
21. E. Z. Faraggi, H. Chayet, D. Davidov, Y. Avny, R. Neumann, *ibid.*, p. 1247.
22. Y. Cao, P. Smith, A. J. Heeger, *ibid.* **48**, 91 (1992).
23. O. T. Ikkala *et al.*, *ibid.* **84**, 55 (1997).
24. J. S. Walker and C. A. Vause, *Sci. Am.* **256**, 98 (May 1987).
25. I. C. Sanchez, *Macromolecules* **24**, 908 (1991).
26. We thank E. L. Thomas for collaboration in electron microscopy at the early stage of this work and M. Saariaho, J. Tanner, and H. Isotalo for experimental assistance and discussions. The Institute of Biotechnology/Electron Microscopy Unit is acknowledged for the privilege of using their facilities. Supported by the Finnish Academy, Technology Development Centre (Finland), and Neste Foundation.

16 December 1997; accepted 3 March 1998

Platinum Catalysts for the High-Yield Oxidation of Methane to a Methanol Derivative

Roy A. Periana,* Douglas J. Taube, Scott Gamble, Henry Taube, Takashi Satoh, Hiroshi Fujii

Platinum catalysts are reported for the direct, low-temperature, oxidative conversion of methane to a methanol derivative at greater than 70 percent one-pass yield based on methane. The catalysts are platinum complexes derived from the bidiazine ligand family that are stable, active, and selective for the oxidation of a carbon-hydrogen bond of methane to produce methyl esters. Mechanistic studies show that platinum(II) is the most active oxidation state of platinum for reaction with methane, and are consistent with reaction proceeding through carbon-hydrogen bond activation of methane to generate a platinum-methyl intermediate that is oxidized to generate the methyl ester product.

More efficient methods for the oxidation of low-value, light alkane feedstocks, such as natural gas, to the corresponding alcohols or other useful liquid products would accelerate the use of natural gas feedstocks as a complement to petroleum. Current technologies for the conversion of natural gas to liquid products proceed by generation of carbon monoxide and hydrogen (syn-gas) that is then converted to higher products through Fischer-Tropsch chemistry (1). The initial formation of syn-gas in these processes is energy intensive and proceeds at high temperatures, typically 850°C. In contrast, direct methods partially oxidize the alkane molecule, functionalizing one C-H bond, and in principle can proceed more efficiently and cost-effectively through lower temperature routes.

Given the potential for high payoff, the goal of direct, selective alkane oxidation has been the focus of substantial effort since the 1970s (2, 3). Despite these extensive efforts, very few selective alkane oxidation processes are known. Except in a few special

cases (4), the basic chemistry for the selective, low-temperature, direct, oxidative conversion of alkane C-H bonds to useful functional groups in high one-pass yield (5) has not yet been developed. Such development is challenging, because alkane C-H bonds are among the least reactive known and the desired products of oxidation are typically more reactive than the starting alkanes and are consumed before recovery. Consequently, only uneconomically low one-pass yields can be obtained with direct alkane oxidation chemistries available today without prohibitively expensive separations and recycle.

We developed a catalytic system for the direct, low-temperature, selective oxidation of methane to generate an ester of methanol in 72% one-pass yield at 81% selectivity based on methane (5). Recently, we reported the selective oxidation of methane to an ester of methanol in ~43% one-pass yield catalyzed by mercuric salts (6). We now show that selected Pt complexes are more effective catalysts for this reaction. These Pt complexes are stable and selectively activate (7) and oxidize a C-H bond of methane at temperatures as low as 100°C to generate a methyl ester product that is chemically "protected" from overoxidation

Catalytica Advanced Technologies Inc., 430 Ferguson Drive, Mountain View, CA 94043, USA.

*To whom correspondence should be addressed. E-mail: rap@mv.catalytica-inc.com